Processing and Application of Ceramics 15 [1] (2021) 79–86
https://doi.org/10.2298/PAC2101079H

Effects of sintering temperature on structure and electrical properties of $(Na_{0.48}K_{0.473}Li_{0.04}Sr_{0.007})(Nb_{0.883}Ta_{0.05}Sb_{0.06}Ti_{0.007})O_3$ piezoelectric ceramics

Cheng-Shong Hong*, Yi-Tian Hong

Department of Electronic Engineering, National Kaohsiung Normal University, Kaohsiung 824, Taiwan, R.O.C.

Received 10 September 2020; Received in revised form 7 December 2020; Aaccepted 24 February 2021

Abstract

In this study, the effects of sintering temperature on microstructure, dielectric and piezoelectric properties are investigated for the non-stoichiometric $(Na_{0.48}K_{0.473}Li_{0.04}Sr_{0.007})(Nb_{0.883}Ta_{0.05}Sb_{0.06}Ti_{0.007})O_3$ (NKLNTS-ST) piezoelectric ceramics. The results suggest that the piezoelectric properties are enhanced owing to the more normal ferroelectric characteristics, higher density, more uniform grains and presence of polymorphic phase transition regions, which are observed with an increase in the sintering temperature up to 1080 °C. The piezoelectric properties are weakened owing to the larger degree of diffuse phase transition and more cation-oxygen-vacancy pairs with an increase in the sintering temperature above 1080 °C. The best piezoelectric properties including k_p = 40%, d_{33} = 288 pC/N, θ_{max} = 72.12, loss = 2.57%, E_c = 13.45 kV/cm and P_r = 10.23 μC/cm^2 are obtained at the sintering temperature of 1080 °C.

Keywords: *lead-free piezoceramics, sintering, phase transition, dielectric and piezoelectric properties*

I. Introduction

Piezoelectric materials can be used in various applications, such as actuators, sensors, transformers, ultrasonic transducers and energy harvester [1]. $Pb(Zr_{1-x}Ti_x)O_3$ (PZT) materials have superior electromechanical properties and performances when morphotropic phase boundaries (MPBs) exist in the piezoelectric ceramics [2,3]. However, the Pb-based ceramics are toxic, cause environmental pollution and affect the human health. Therefore, eco-friendly materials have been fabricated in recent years [4]. Among the various lead-free piezoelectric materials, the sodium potassium niobate $(Na_{1-x}K_x)NbO_3$ (NKN) ceramics exhibits an outstanding piezoelectric coefficient d_{33} of 97 pC/N and high Curie temperature of 420 °C [3,5,6]. However, synthesis and sintering of NKN-based materials are challenging. Owing to the high sintering temperature (1100 °C), Na and K cations easily volatilize at high temperatures and thus it is difficult to obtain a high density (4.25 g/cm^3) and high electromechanical coupling factor (k_p = 25–35%) [3,5,6]. Therefore, extensive studies have been carried out on the $(Na_{0.5}K_{0.5})NbO_3$ ceramic system by doping with different elements, which can improve densification during the sintering and overcoming the problem of easy deliquescence [7,8].

Lim *et al.* [9] and Feng *et al.* [10] reported that the piezoelectricity also increases by incorporation of different dopants in the NKN ceramic structure as polymorphic phase boundaries (PPBs - coexistence of the orthorhombic and tetragonal phases) can be obtained at room temperature. Kim *et al.* [11] reported that the electrical properties were improved and that the orthorhombic to tetragonal phase-transition temperature T_{O-T} was decreased to room temperature when lithium, tantalum and antimony were added. The presence of PPBs can induce good electric properties, similar to the MPBs in lead-based piezoelectric ceramics [2,3]. Lin *et al.* [12] reported that the densities and piezoelectric properties of NKN-based ceramics can be improved by substituting Li, Ta, and Sb at A and B sites of $(1-x)K_{0.5}Na_{0.5}(Nb_{0.94}Sb_{0.06})O_3$-$xLiTaO_3$ ceramics with excellent piezoelectric properties including d_{33} = 271 pC/N and k_p = 53% at room temperature. Furthermore, Chang *et al.* [13] reported that the piezoelectric

*Corresponding authors: tel: +886 7 7172930 / 7915,
e-mail: *cshong@nknu.edu.tw*

properties were enhanced and the loss tangents were reduced through Sr^{2+} and Ti^{4+} ions in NKN-based ceramics. Su *et al.* [14] reported excellent piezoelectric properties owing to the PPBs in non-stoichiometric $(Na_{0.48}K_{0.473}Li_{0.04}Sr_{0.007})(Nb_{0.883}Ta_{0.05}Sb_{0.06}Ti_{0.007})O_3$ (NKLNTS-ST) piezoelectric ceramics (bulk type) fabricated by using the conventional solid-state reaction method. However, the effects of the sintering temperature on the NKLNTS-ST piezoelectric ceramics have not been analysed.

The multi-layer technology based on tape casting has an important role for the fabrication of these structures. The thinner film and the textured ceramics are usually fabricated by tape casting technology. However, its electric property is inferior to bulk ceramics because of less density and grain growth. Therefore, in this study applicability of tape casting for processing of the non-stoichiometric NKLNTS-ST piezoelectrics is evaluated. The effects of sintering temperature are also investigated. In addition, the dielectric properties of the obtained NKLNTS-ST ceramics are estimated by using the empirical and Curie-Weiss laws. The piezoelectric properties are also analysed by the resonant frequency method and ferroelectric hysteresis loops.

II. Experimental methods

2.1. Sample preparation

Na_2CO_3, K_2CO_3, Li_2CO_3, $SrCO_3$, Nb_2O_5, Sb_2O_3, Ta_2O_5 and TiO_2 powders (purity: >99%) were used as raw materials to fabricate the non-stoichiometric NKLNTS-ST ceramics by tape casting. First, Na_2CO_3, K_2CO_3, Li_2CO_3, $SrCO_3$, Nb_2O_5, Sb_2O_3, Ta_2O_5 and TiO_2 powders were ball-milled together with ZrO_2 balls in a polyethylene jar for 24 h using ethanol (purity: 99%) as the medium. The slurry was dried and then calcined at 890 °C in air for 4 h. The calcined powders were thoroughly mixed with a solvent (50 vol.% ethanol and 50 vol.% toluene) and dispersant in a ball mill for 24 h. A binder and plasticizer were added and then the mixture was ball-milled again for 24 h. The slurry was tape-cast to form a green sheet with a thickness of approximately 30 μm on an aluminium foil by using a doctor blade apparatus. After drying, a single-layer sheet was cut, fifteen layers were laminated, and then hot-pressed at temperature of 60 °C and pressure of 80 MPa for 5 min to form a 0.5 mm thick green sheet. The laminated green sheets were heated at 600 °C for 10 h with an intermediate step at 300 °C for 5 h to remove organic substances before sintering. The samples were sintered in air at different temperatures (1060–1140 °C) for 3 h, and then cooled to room temperature at a cooling rate of 5 °C/min. Silver paste was fired on the surfaces at 750 °C for 20 min to obtain electrodes for the measurement of electrical properties. The samples were then poled in silicon oil at 60 °C for 20 min under a direct-current field of 3 kV/mm. The piezoelectric properties were measured after the poling for 24 h.

2.2. Measurements

The densities of the sintered samples were measured by using the Archimedes' method. The phase relations of the sintered samples were identified by XRD (D2 PHASER, Bruker, Germany) with Cu K_α radiation (λ = 0.154 nm). The microstructures were observed by using scanning electronic microscopy (field-emission SEM, SU8000, Hitachi, Japan). The dielectric constants (in the range of 25 to 450 °C at 1 MHz) and piezoelectric properties were measured by using a precision impedance analyser (4294A, HP, USA). The piezoelectric constant d_{33} was measured at room temperature by utilizing a static piezoelectric-constant testing meter (APC Cat. #90-2030). The *P-E* hysteresis loops were measured by using a ferroelectric tester at 1 Hz (Precision Premier II Ferroelectric Tester, Radiant Technology).

III. Results and discussion

3.1. XRD patterns and analysis

Figure 1a shows XRD patterns of the NKLNTS-ST ceramics sintered at different temperatures. Silicon powders are used for calibration to obtain exact diffraction angles. All samples exhibit almost pure perovskite structures without obvious secondary phases, similar to previous results [14]. The split phenomenon occurs as the lattice structure is transformed to a structure in which orthorhombic (002) and tetragonal (200) phases coexist [15], as shown in Fig. 1b. When the sintering temperature of the sample increases, it is found that the shift of the peak to the right means that the crystal lattice becomes smaller (Fig. 1b). The ionic radius of Sr (Sr^{2+} = 1.18 Å) at A-site and the ionic radius of Ti (Ti^{2+} = 0.60 Å) at B-site are smaller than those of K (K^+ =

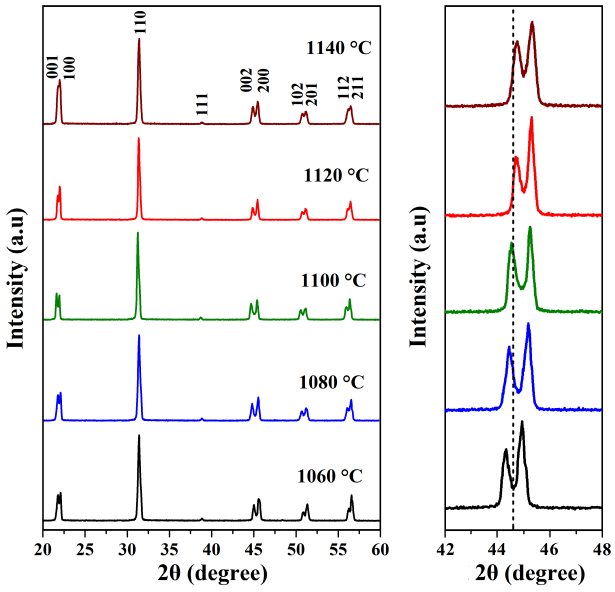

Figure 1. XRD patterns of the NKLNTS-ST ceramics sintered at different temperatures (a) and expanded XRD patterns in the 2θ range of 42–48° (b)

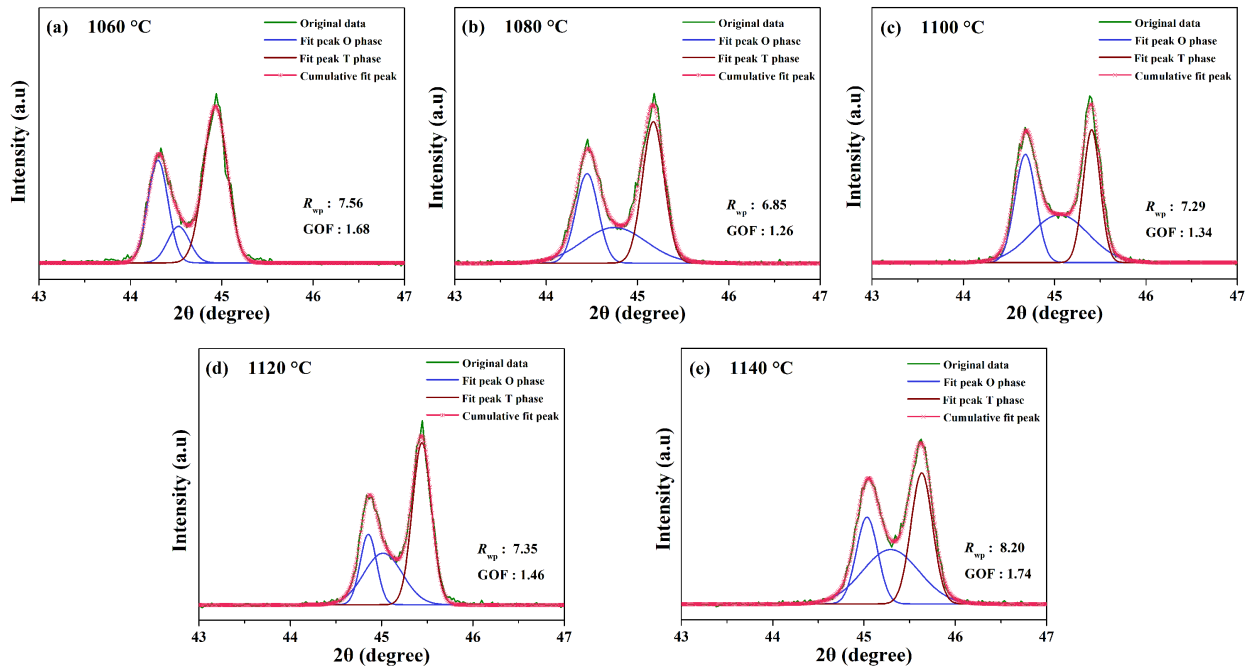

Figure 2. The (002)-(200) XRD peaks and their fitting results for the NKLNTS-ST ceramics sintered at: a) 1060, b) 1080, c) 1100, d) 1120 and e) 1140 °C

1.30 Å) and Nb (Nb^{5+} = 0.64 Å), Ta (Ta^{5+} = 0.64 Å), Sb (Sb^{5+} = 0.61 Å) ion radii. Therefore, it is suggested that the solid solubility is enhanced with increasing the sintering temperature. Furthermore, the observed shifting of the XRD peaks to the right could be also due to the alkaline elements volatilization because of its low volatilization temperature.

In Fig. 1, only two XRD peaks corresponding to (002) and (200) plains are clearly seen. In order to further examine the changes in the diffraction peaks Rietveld refinement software was employed for the XRD 2θ range from 43° to 47° and the fitting results are shown in Fig. 2. It is found that the samples at different sintering temperatures have coexisting orthorhombic (O phase) and tetragonal (T phase) phases with three XRD peaks. Furthermore, the calculated weighted-profile *R*-factor (R_{wp}) and goodness of fit (*GOF*) have very small values. Usually R_{wp} needs to be less than 10% and *GOF* needs to be less than 4% [16], which demonstrates that the fitting results can accurately describe the measured XRD patterns. The weighted ratio of orthorhombic and tetragonal phases changes with the increase of sintering temperature, as shown in Fig. 3. When the sintering temperature increases to 1080 °C, the amounts of O and T phases are quite close. This suggests the presence of polymorphic phase transition (PPT) regions in the NKLNTS-ST ceramics. As the sintering temperature continues to increase to 1120–1140 °C the content of O and T phases changes again. Li *et al.* [17] reported that during high sintering temperature processing of NKN-based piezoceramics oxygen vacancies are generated because of the volatile nature of the alkali elements (sodium/potassium). In conclusion, the phase structures are affected by the $SrTiO_3$ (ST) content and

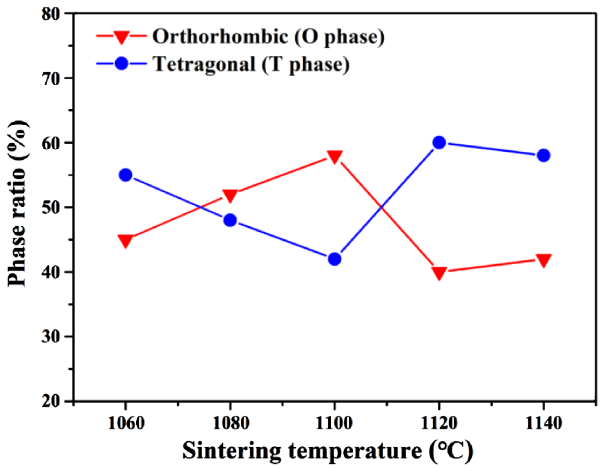

Figure 3. Phase structure transitions of the NKLNTS-ST ceramics sintered at different temperatures

the alkali-oxygen vacancy pairs. At the lower sintering temperatures 1060–1100 °C, the amount of O phase is increased and T phase is decreased since sintering in this temperature range enhances the solid solution for the NKLNTS-ST ceramics. At higher sintering temperatures 1120–1140 °C, the amount of O phase is decreased and T phase is increased since the alkali-oxygen vacancy pairs are induced by the volatilization of the alkali elements.

3.2. Densities

Figure 4 shows the densities of the NKLNTS-ST ceramics sintered at different temperatures, which are estimated by using the Archimedes method. As shown in Fig. 4, the maximum density of 4.66 g/cm^3 is obtained at the sintering temperature of 1080 °C. According to the

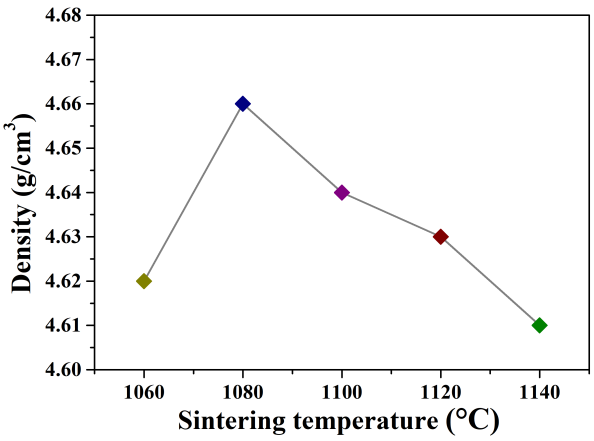

Figure 4. Phase structure transitions of the NKLNTS-ST ceramics sintered at different temperatures

SEM images (Fig. 5), this is attributed to the increase in grain size and decrease in pore content with the increase in sintering temperature. The density decreases with the increase in sintering temperature above 1080 °C. These results are similar to those reported by Kim *et al.* [11], Cen *et al.* [19] and Palei *et al.* [20] who confirmed that the alkaline elements easily volatilize and form cation vacancies in NKN-based ceramics when the sintering temperature is too high. Thus, the low density at the increased sintering temperature is attributed to the volatilized alkaline elements and increased pore content, as shown in SEM images (Fig. 5).

3.3. SEM analyses

Figure 5 shows SEM images of the NKLNTS-ST ceramics sintered at different temperatures. No obvious secondary phases are observed for all samples, consistent with the XRD results (Fig. 1). The grain size distribution is uniform, while the grains have square shapes, similar to the previous results [18–20]. As shown in Fig. 5a, the grain size is small and more pores are observed when the lowest sintering temperature of 1060 °C is used. The grain size increases, while pore content decreases with the increase in sintering temperature. However, pore content seems to increase again when the sintering temperature is sufficiently high. The average grain sizes of the samples sintered at different temperatures of 1060, 1080, 1100, 1120 and 1140 °C, estimated by using the log-normal size distribution model [21], are 1.2, 1.5, 1.8, 2.4 and 3.3 μm, respectively (Fig. 5).

3.4. Dielectric properties

Figure 6 shows the 1 MHz dielectric constants versus temperature of the NKLNTS-ST ceramics sintered at different temperatures. As shown in Fig. 6a, the dielectric peak is broad at the sintering temperature of 1060 °C, while that at 1080 °C is narrow. However, the broadening of the dielectric peak is increased again at sintering temperatures higher than 1080 °C, similar to previous results [18]. The broad dielectric peak represents the diffuse phase transition [22,23]. Typically, the degree of diffuse phase transition (DPT) is expressed as [24]:

$$\varepsilon = \frac{\varepsilon_m}{1 + \left(\frac{T - T_m}{D}\right)^{\xi}} \tag{1}$$

where ε_m is the maximum dielectric constant at the temperature T_m, ξ is a diffusion parameter (in the range of 1 to 2; normal ferroelectric characteristics are observed at ξ value of approximately 1, while total DPT relaxor characteristics are observed at ξ value of approximately 2 [25]), and D is the diffusion extension (a larger D implies more diffusive characteristics [25]).

The experimental data in Fig. 6 are fitted by using Eq. 1. The fitting results are consistent with the experimental data, as the measurement temperature is only in the paraelectric area (after the peak), similar to previ-

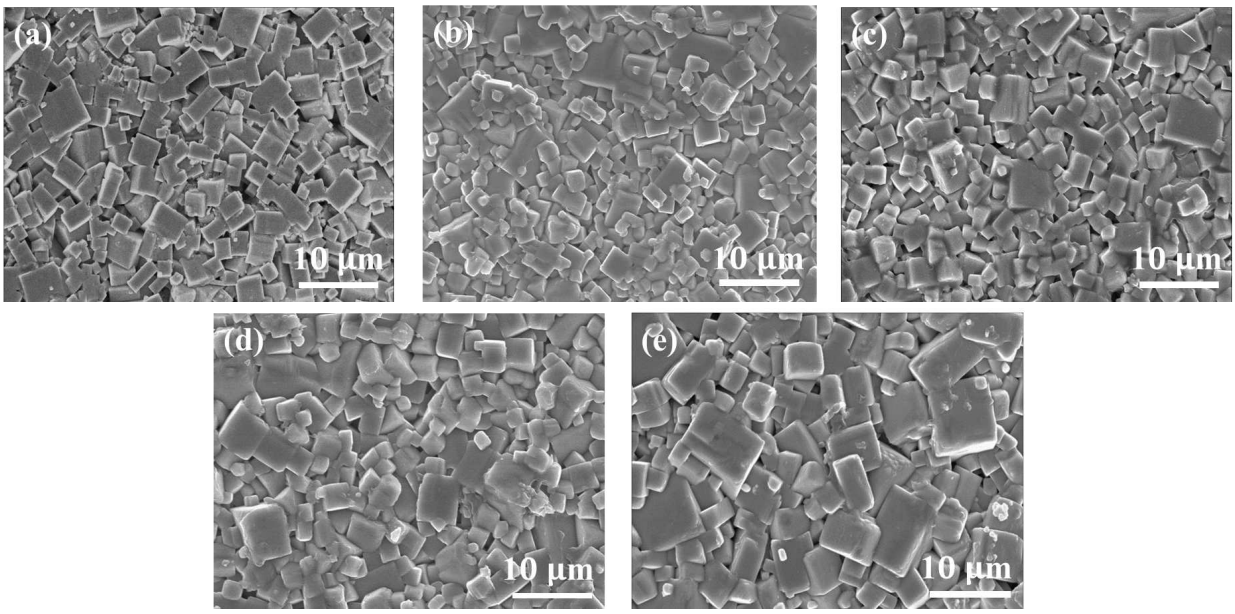

Figure 5. SEM images of the NKLNTS-ST ceramics sintered at: a) 1060, b) 1080, c) 1100, d) 1120 and e) 1140 °C

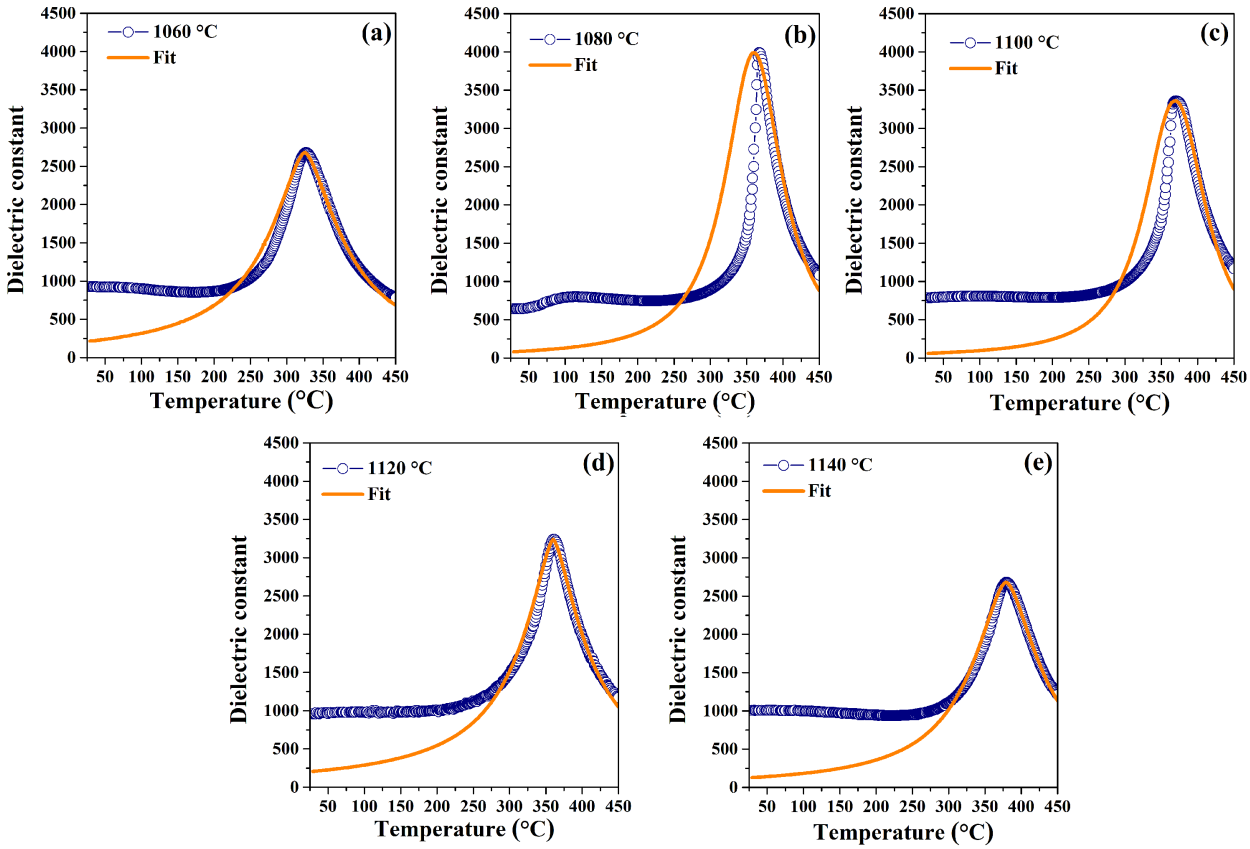

Figure 6. Measured and fitted dielectric constants of the NKLNTS-ST ceramics sintered at: a) 1060, b) 1080, c) 1100, d) 1120 and e) 1140 °C as functions of the temperature

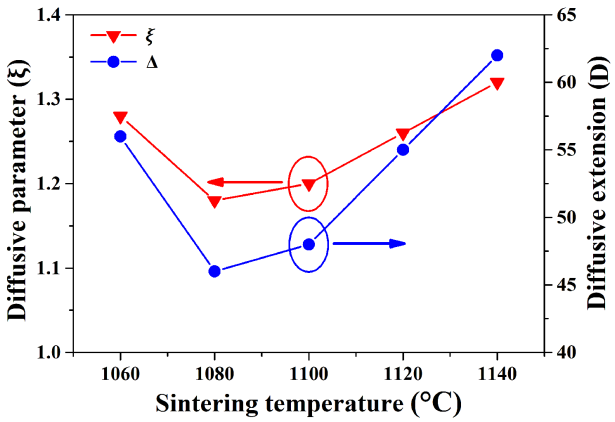

Figure 7. Phase structure transitions of the NKLNTS-ST ceramics sintered at different temperatures

ous results [23]. According to work done by Santos and Eiras [24] and Clarke and Burfoot [25], the empirical law can be used to describe the dielectric behaviour of the paraelectric area of a material.

According to the fitting results in Fig. 6, the DPT behaviour (ξ and D values) can be estimated as shown in Fig. 7. The ξ and D values increase with a decrease in sintering temperature up to 1080 °C. Above 1080 °C, the ξ and D values increase with an increase in the sintering temperature, similar to previous results [18]. Hao *et al.* [26] reported that the short-range order and DPT relaxor behaviour start to be more significant as the small grains lead to domain refinement in the $(Ba_{0.85}Ca_{0.15})(Zr_{0.1}Ti_{0.9})O_3$ lead-free piezoelectric ceramics. Furthermore, the alkaline elements easily volatilize in NKN-based ceramics when the sintering temperature is sufficiently high [14]. Therefore, the dielectric behaviour is affected owing to the induced cation-oxygen-vacancy pairs [27]. The experimental results in Fig. 7 and previous reports suggest that the long-range order and normal ferroelectric characteristic are enhanced owing to the larger grain size when the sintering temperature is increased. Furthermore, the DPT is increased with increasing content of cation-oxygen-vacancy pairs when the sintering temperature is sufficiently high.

The Curie-Weiss law is also usually used to describe the dielectric behaviour, which was proposed to explain the phase transitions of ferromagnetic materials. The paramagnetic phase is observed above the Curie temperature (T_C), while spontaneous polarization is induced when the temperature is below T_C. A large number of studies have demonstrated that the dielectric behaviour follows the Curie-Weiss law [28,29]:

$$\chi = \frac{C}{T - \theta} \tag{2}$$

where χ is the dielectric susceptibility, C is the Curie-Weiss constant, and θ is the Curie-Weiss temperature, slightly lower than the phase transition temperature T_m

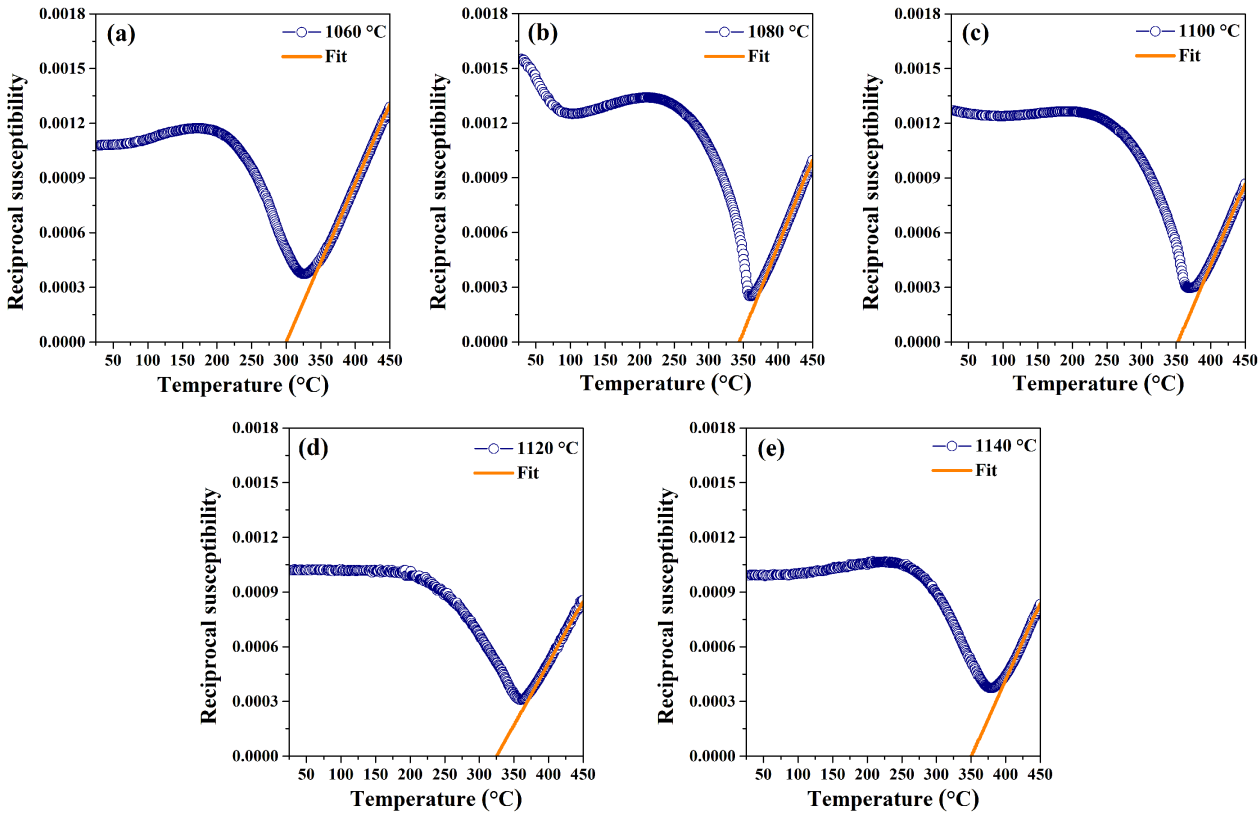

Figure 8. Temperature dependences of the reciprocal dielectric constants and curves fitted by using the Curie-Weiss law for the NKLNTS-ST ceramics sintered at: a) 1060, b) 1080, c) 1100, d) 1120 and e) 1140 °C

corresponding to the maximum dielectric constant. Figure 8 shows the 1 MHz reciprocal dielectric susceptibilities of the NKLNTS-ST ceramics sintered at various temperatures as a function of the temperature and their fitting curves according to the Curie-Weiss law. As shown in Fig. 8, the dielectric behaviour follows the Curie-Weiss law when the measurement temperature is sufficiently high in the paraelectric range. When the measurement temperature is decreased and is close to the phase transition temperature T_m, the dielectric behaviour deviates from the Curie-Weiss law. The temperature at which the deviation begins is denoted as T_B. The deviation is induced by the correlation of neighbouring polar microregions or freezing of spontaneous polar pairs. The deviation is dependent on the DPT [30]. Therefore, the empirical parameter ΔT_m is usually used to estimate the degree of deviation from the Curie-Weiss law [31]:

$$\Delta T_m = T_B - T_m \tag{3}$$

Table 1 shows the ΔT_m, T_B and T_m values obtained according to the experimental data and fitting by Eqs. 2 and 3. As shown in Table 1 and Fig. 8, the ΔT_m values and DPTs are lower at sintering temperatures of 1080 and 1100 °C. In contrast, the ΔT_m values are higher, while the DPTs are larger at sintering temperatures of 1060, 1120 and 1140 °C. These results are consistent with previous results [18].

3.5. *Piezoelectric and ferroelectric properties*

Figure 9 shows the piezoelectric properties (k_p, d_{33}, θ_{max} and loss) of the NKLNTS-ST ceramics sintered at various temperatures. The piezoelectric properties are enhanced when the sintering temperature is increased. The best piezoelectric properties (k_p = 40%, d_{33} = 288 pC/N, θ_{max} = 72.12, loss = 2.57%) are observed at the sintering temperature of 1080 °C. With the increase in sintering temperature above 1080 °C, the piezoelectric properties weaken, similar to the previous results [18]. According to the experimental data and previous reports, the piezoelectric properties are dependent on the normal ferroelectric characteristics, density and grain uniformity [10]. The more normal ferroelectric characteristics, higher density and more uniform grains can enhance the piezoelectric properties with the increase in sintering temperature up to 1080 °C [10]. The

Table 1. Empirical parameters of the NKLNTS-ST ceramics sintered at different temperatures

Sintering temperature [°C]	1060	1080	1100	1120	1140
T_B [°C]	380	390	398	411	435
T_m [°C]	326	350	355	360	379
ΔT_m [°C]	56	40	43	51	59

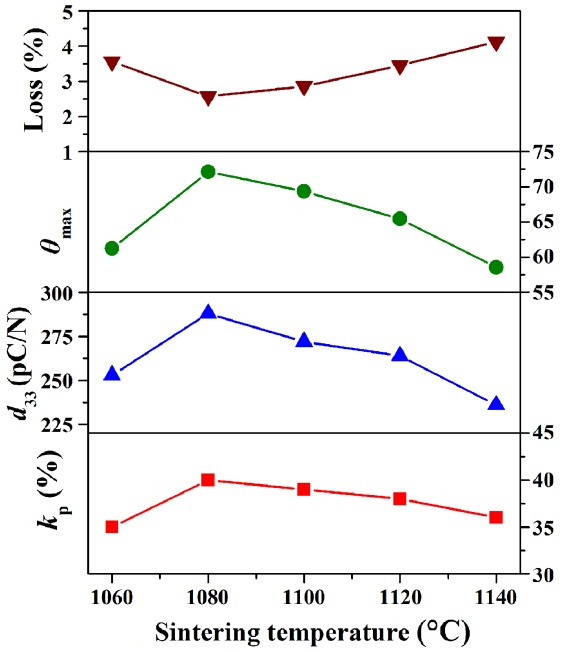

Figure 9. Piezoelectric parameters of the NKLNTS-ST ceramics sintered at different temperatures

larger DPT and number of cation-oxygen-vacancy pairs can weaken the piezoelectric properties with the increase in sintering temperature above 1080 °C [14,27].

Figure 10 shows the polarization-electric-field (*P-E*) hysteresis loops of the NKLNTS-ST ceramics (sintered at different temperatures) at room temperature at a frequency of 1 Hz. The ferroelectric hysteresis loops significantly change with an increase in the sintering temperature. At lower sintering temperatures, the shape of the hysteresis loop changed from thinner to thicker with an increase in the sintering temperature. The thickest hysteresis loop is observed at the sintering temperature of 1080 °C. The maximum remnant polarization P_r and maximum coercive electric field E_c are 10.23 μC/cm^2 and 13.45 kV/cm, respectively, at the sintering temperature of 1080 °C, as shown in Fig. 11. At sintering temperatures higher than 1080 °C, the hysteresis loop

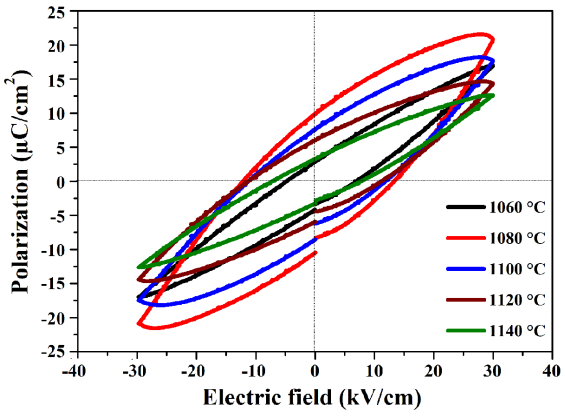

Figure 10. Ferroelectric hysteresis loops (*P-E*) of the NKLNTS-ST ceramics sintered at different temperatures measured at 1 Hz at room temperature

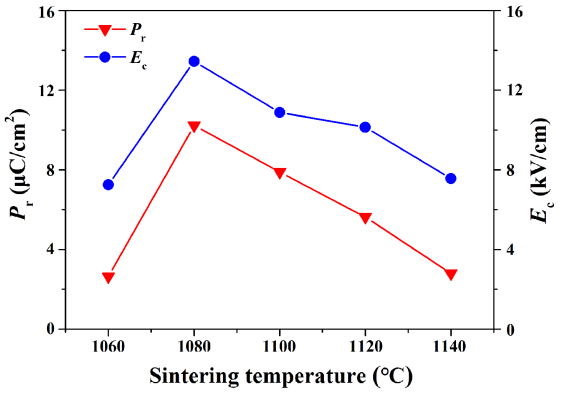

Figure 11. Remnant polarization (P_r) and coercive electric field (E_c) of the NKLNTS-ST ceramics sintered at different temperatures

changed from thicker to thinner with an increase in the sintering temperature, similar to the previous results [20]. The reason is that the density and grain size increase as the sintering temperature increases. The increase in P_r of the NKLNTS-ST samples sintered at 1080 °C may be related to the increase in domain wall motion and the increase in grain size, which helps to switch domains and therefore affects the amount of polarization [32]. With the further increase of the sintering temperature, the value of P_r is found to decrease, which may be due to the increase of the grain size, which leads to the decrease of density due to excessive extrusion. According to the experimental data and previous reports, the hysteresis loops are dependent on the DPT. A relaxor ferroelectric with a larger DPT has a thinner hysteresis loop [33].

IV. Conclusions

In this study, we investigated the effects of the sintering temperature on the non-stoichiometric NKLNTS-ST ceramics. All samples exhibited pure perovskite structure. The dielectric behaviour and piezoelectric properties changed with the sintering temperature. The best piezoelectric and ferroelectric properties including k_p = 40%, d_{33} = 288 pC/N, θ_{max} = 72.12, loss = 2.57%, E_c = 13.45 kV/cm and P_r = 10.23 μC/cm^2 were obtained at the sintering temperature of 1080 °C. The better piezoelectric properties could be attributed to higher density, more uniform grains, smaller number of cation-oxygen-vacancy pairs, more normal ferroelectric characteristics and presence of polymorphic phase transition regions.

Acknowledgements: This research was supported by the Ministry of Science and Technology (MOST), Taiwan, R.O.C., under grant MOST 106-2221-E-017-010-MY3.

References

1. B. Jaffe, W.R. Cook, H.L. Jaffe, *Piezoelectric Ceramics*, Academic Press, New York, 1971.

2. S. Hu, C. Luo, P. Li, J. Hu, G. Li, H. Jiang, W. Zhang, "Effect of sintered temperature on structural and piezoelectric properties of barium titanate ceramic prepared by nano-scale precursors", *J. Mater. Sci. Mater. Electron.*, **28** (2017) 9322–9327.
3. Y. Guo, K.I. Kakimoto, H. Ohsato, "Phase transitional behavior and piezoelectric properties of $(Na_{0.5}K_{0.5})NbO_3$-$LiNbO_3$ ceramics", *Appl. Phys. Lett.*, **85** (2004) 4121.
4. L. Gao, S. Dursun, A.E. Gurdal, E. Hennin, S. Zhang, C.A. Randall, "Atmospheric controlled processing enabling highly textured NKN with enhanced piezoelectric performance", *J. Eur. Ceram. Soc.*, **39** (2019) 963–972.
5. P. Li, J. Zhai, B. Shen, S. Zhang, X. Li, F. Zhu, X. Zhang, "Ultrahigh piezoelectric properties in textured (K,Na)NbO_3-based lead-free ceramics", *Adv. Mater.*, **30** (2018) 1705171.
6. R. Zuo, C. Ye, X. Fang, "$Na_{0.5}K_{0.5}NbO_3$-$BiFeO_3$ lead-free piezoelectric ceramics", *J. Phys. Chem. Solids*, **69** (2008) 230–235.
7. X. Li, B. Fan, H. Jia, X. Shi, Y. Zhang, X. Yang, R. Zhang, "Structure and piezoelectric properties of $CaZrO_3$-modified (K,Na,Li)(Nb,Sb)O_3 ceramics prepared from powders synthesized by microwave heating", *Process. Appl. Ceram.*, **13** [4] (2019) 368–375.
8. J.J. Zhou, L.Q. Cheng, K. Wang, X.W. Zhang, J.F. Li, H. Liu, J.Z. Fang, "Low-temperature sintering of (K,Na)NbO_3-based lead-free piezoceramics with addition of LiF", *J. Eur. Ceram. Soc.*, **5** (2014) 1161–1167.
9. J.B. Lim, S. Zhang, J.H. Jeon, T.R. Shrout, "(K,Na)NbO_3-based ceramics for piezoelectric hard lead-free materials", *J. Am. Ceram. Soc.*, **93** (2010) 1218–1220.
10. W. Feng, H. Du, C. Chen, Y. Huang, X. Tan, "Electric-field-driven phase transition process in (K,Na,Li)(Nb,Ta,Sb)O_3 lead-free piezoceramics", *J. Am. Ceram. Soc.*, **99** (2016) 135–140.
11. J. Kim, J.H. Ji, J.H. Koh, "Improved Li and Sb doped lead-free (Na,K)NbO_3 piezoelectric ceramics for energy harvesting applications", *Ceram. Int.*, **44** (2018) 22219–22224.
12. D. Lin, K.W. Kwok, K.H. Lam, H.L.W. Chan, "Phase structure and electrical properties of $K_{0.5}Na_{0.5}(Nb_{0.94}Sb_{0.06})O_3$-$LiTaO_3$ lead-free piezoelectric ceramics", *J. Phys. D Appl. Phys.*, **41** (2008) 052002.
13. R.C. Chang, S.Y. Chu, Y.P. Wong, C.S. Hong, H.H. Huang, "The effects of sintering temperature on the properties of lead-free $(Na_{0.5}K_{0.5})NbO_3$-$SrTiO_3$ ceramics", *J. Alloy. Compd.*, **456** (2008) 308–312.
14. H.H. Su, C.S. Hong, C.C. Tsai, S.Y. Chu, "Relaxor behavior of lead-free nonstoichiometric $(Na_{0.48-x}K_{0.48-x}Li_{0.04})Nb_{0.89-x}Ta_{0.05}Sb_{0.06}O_3$-$x$$SrTiO_3$ ceramics", *ECS J. Solid State Sci. Technol.*, **6** (2017) N117–N121.
15. K. Wang, J.F. Li, "Domain engineering of lead-free Li-modified (K,Na)NbO_3 polycrystals with highly enhanced piezoelectricity", *Adv. Funct. Mater.*, **20** (2010) 1924–1929.
16. Y. Liao, D. Wang, H. Wang, T. Wang, Q. Zheng, J. Yang, K.W. Kwok, D. Lin, "Transformation of hardening to softening behaviors induced by Sb substitution in CuO-doped KNN-based piezoceramics", *Ceram. Int.*, **45** (2019) 13179–13186.
17. J.F. Li, K. Wang, "Ferroelectric and piezoelectric properties of fine-grained $Na_{0.5}K_{0.5}NbO_3$ lead-free piezoelectric ceramics prepared by spark plasma sintering", *J. Am. Ceram. Soc.*, **89** (2006) 706–709.
18. H.H. Su, C.S. Hong, C.C. Tsai, S.Y Chu., H.R. Chen, Y.D. Juang, "Phase structure transformations and electrical properties of $(Na_{0.52}K_{0.4425})(Nb_{0.8925}Sb_{0.07})O_3$-$0.0375LiTaO_3$ ceramics according to sintering temperature", *ECS J. Solid State Sci. Technol.*, **7** (2018) N29–N35.
19. Z. Cen, Y. Zhen, W. Feng, P. Zhao, L Chen., X. Wang, L. Li, "Sintering temperature effect on microstructure, electrical properties and temperature stability of MnO-modified KNN-based ceramics", *J. Eur. Ceram. Soc.*, **38** (2018) 3136–3146.
20. P.K. Palei, P. Kumar, "Role of sintering temperature on the phase stability and electrical properties of $0.94(K_{0.5}Na_{0.5}NbO_3)$-$0.06(LiSbO_3)$ ceramics", *Jpn. J. Appl. Phys.*, **51** (2012) 011503.
21. J. Heintzenberg, "Properties of the log-normal particle size distribution", *Aerosol Sci. Technol.*, **21** [1] (1994) 46–48.
22. Q. Xu, Z. Li, "Dielectric and ferroelectric behaviour of Zr-doped $BaTiO_3$ perovskites", *Process. Appl. Ceram.*, **14** [3] (2020) 188–194.
23. Z. Xu, S.M. Gupta, D. Viehland, "Direct imaging of atomic ordering in undoped and La-doped $Pb(Mg_{1/3}Nb_{2/3})O_3$", *J. Am. Ceram. Soc.*, **83** (2000) 181–188.
24. I.A. Santos, J.A. Eiras, "Phenomenological description of the diffuse phase transition in ferroelectrics", *J. Phys. Condes. Matter*, **13** (2001) 11733–11740.
25. R. Clarke, J.C. Burfoot, "The diffuse phase transition in potassium strontium niobate", *Ferroelectrics*, **8** (1974) 505–506.
26. J. Hao, W. Bai, W. Li, J. Zhai, C. Randal, "Correlation between the microstructure and electrical properties in high-performance $(Ba_{0.85}Ca_{0.15})(Zr_{0.1}Ti_{0.9})O_3$ lead-free piezoelectric ceramics", *J. Am. Ceram. Soc.*, **95** (2012) 1998–2006.
27. J. Yoo, "Effect of sintering temperature on the dielectric and piezoelectric properties of $(Na_{0.525}K_{0.443}Li_{0.037})(Nb_{0.883}Sb_{0.08}Ta_{0.037})O_3$ Pb-free ceramics for actuator", *Ferroelectrics*, **507** (2017) 12–18.
28. L.L. Hench, J.K. West, *Principles of Electronic Ceramics*, John Wiley & Sons, New York, 1989.
29. K. Uchino, *Ferroelectric Devies*, Marcel Dekker, New York, 2000.
30. D. Viehland, S.J. Jang, L.E. Cross, M. Wutting, "Deviation from Curie-Weiss behavior in relaxor ferroelectrics", *Phys. Rev. B*, **46** (1992) 8003.
31. C.S. Hong, S.Y. Chu, W.C. Su, R.C. Chang, H.H. Nien, Y.D. Juang, "The sintering temperature-induced transition from relaxor to ferroelectric in $0.7PbFe_{2/3}W_{1/3}O_3$-$0.3PbTiO_3$ ceramics", *J. Alloy. Compd.*, **459** (2008) 1–7.
32. P. Kumar, P. Palei, "Effect of sintering temperature on ferroelectric properties of $0.94(K_{0.5}Na_{0.5})NbO_3$-$0.06LNbO_3$ system", *Ceram. Int.*, **36** (2010) 1725–1729.
33. Z. Yang, H. Du, L. Jin, P. Zhao, Q. Hu, S. Qu, Z. Yang, Y. Yu, X. Wei, Z. Xu, "A new family of sodium niobate-based dielectrics for electrical energy storage applications", *J. Eur. Ceram. Soc.*, **38** (2019) 2899–2907.